THE JOURNAL OF PHYSICAL CHEMISTRY C

pubs.acs.org/JPCC Article

Exploring the Role of Vinylene Carbonate in the Passivation and Capacity Retention of Cu_2Sb Thin Film Anodes

Leslie A. Kraynak, Jacob D. Schneider, and Amy L. Prieto*

Cite This: J. Phys. Chem. C 2020, 124, 26083−26093 Read Online

ABSTRACT: Electrolyte additives such as vinylene carbonate (VC) have been demonstrated to improve the capacity retention for many types of Li-ion battery electrodes, including intermetallic alloying anodes. However, it is still unclear why VC extends the cycle lifetime of copper antimonide (Cu_2Sb) anodes so dramatically. Here, we have studied how VC affects the solid electrolyte interface formed on Cu_2Sb thin film anodes in fluorine-free electrolyte solutions in order to better understand which nonfluorinated species may play an important role in effective Cu_2Sb passivation using differential capacity analysis and X-ray photoelectron spectroscopy. We have found that VC effectively passivates Cu_2Sb and prevents Cu/Cu_2Sb oxidation at high potentials. Carbonate species from the reduction of VC seem to play an important role in passivation, while inorganic species like $LiClO_4$ from the F-free supporting electrolyte do not seem to be beneficial.

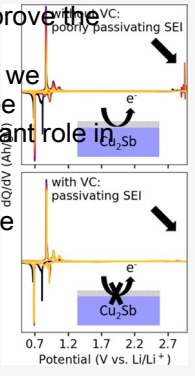

INTRODUCTION

Many research efforts in the energy storage field have been focused on increasing the energy density of the anode materials used in secondary battery technologies such as lithium-ion batteries.[1,2] Lithium alloying materials such as silicon, tin, antimony, and intermetallics have garnered interest as alternative anode materials to replace graphite, a lithium intercalation anode, due to their large theoretical gravimetric and volumetric capacities.[2,3] However, these materials suffer from problems such as large irreversible capacities and short cycle lifetimes.[3] One contributing factor is the large volume change associated with lithiation and delithiation of these materials, which leads to cracking, pulverization, and loss of electrical contact of the anode.[3] Interfacial problems associated with the solid electrolyte interface (SEI) also contribute to the issues associated with these anode materials.[3,4]

The SEI plays an important role in battery performance, affecting the anode irreversible capacity, cycle lifetime, self-discharge, rate capability, and safety, making it a crucial component in lithium-ion batteries.[5,6] It forms on Li-ion battery anodes due to the instability of the liquid electrolyte over the potential window where rechargeable batteries operate.[6−8] The heterogeneous, amorphous film, composed of the decomposition products of organic carbonate solvents and the lithium supporting electrolyte, is difficult to characterize due to its heterogeneity, reactivity to air and moisture, and sensitivity to many variables.[6,9] Variables that can influence the SEI formation, composition, and properties include cycling conditions,[9,10] electrolyte composition,[11−15] and anode composition and fabrication.[16−22]

Much of the battery community's understanding of the SEI comes from studies of the SEI on graphite anodes.[6] However, it is crucial to study the SEI on next generation alloying and conversion anode materials because while the SEI formed on graphite is relatively stable, the large volume changes associated with cycling alloying anodes mean that the SEI forms throughout the cycling process as new electrode surfaces are exposed due to cracking.[3,23] As such, the requirements of the SEIs formed on these anode materials are different than those of graphite.[5,23] In addition to passivating the electrode surface and allowing for good Li$^+$ conduction, a stable SEI on high capacity anodes would also be robust enough to accommodate large volume changes.[5,16] Studies of the SEI formed on Si have contributed to the understanding of SEI formation on alloying anodes, but there is still much to be learned about the SEI on metallic and intermetallic alloying electrode materials.[10,14,15,17,24−26] For Cu_2Sb electrodes in particular, there has been some preliminary characterization of the SEI formed on Cu_2Sb in order to better understand changes in capacity retention and cycle life,[27−29] but there is still much that is unknown due to the lack of comprehensive studies.

Intermetallic electrodes, such as SnSb, AlSb, and Cu_2Sb, are particularly attractive materials for SEI studies not only

Received: May 6, 2020
Revised: October 15, 2020
Published: November 18, 2020

https://dx.doi.org/10.1021/acs.jpcc.0c04064
J. Phys. Chem. C 2020, 124, 26083−26093

because of the dearth of knowledge of intermetallic SEI formation and composition but also because these materials have interesting chemistries that could enrich fundamental knowledge of the SEI. The variety of metallic elements, both active and inactive toward lithium alloying, that make up intermetallic anode materials results in varying surface reactivities and different lithiation/delithiation reactions and potentials.[4,30−33] Additionally, intermetallic electrodes can be prepared without additives or binders via electrodeposition and physical vapor deposition methods.[27,34−36] This makes these anodes ideal candidates for fundamental SEI studies because binders and conductive additives can affect SEI formation, complicating studies of SEI formation and composition.[19−21,37,38] Another advantage of electrodeposition in particular as a fabrication method for intermetallic anodes is that it enables both 2D and 3D anode morphologies, which are a useful synthetic control to have for interfacial studies where an increased surface area may be desired.[29,34,39]

One route to stabilize the SEI is to use small amounts of electrolyte additives such as fluoroethylene carbonate (FEC) and vinylene carbonate (VC).[40] Surprisingly, even though these additives were initially found to improve the SEI on graphite anodes, they also result in dramatically improved cycle lifetimes for alloying anodes.[15,29,40,41] There are many hypotheses about why these additives work so well for all types of anode materials. The prevailing hypothesis is that they behave as a sacrificial component that is reduced before the other electrolyte components to help passivate the electrode surface and prevent excessive SEI formation,[40,41] although computational work suggests that additives like VC may help by altering the reduction pathways of the carbonate solvents.[42] Studies on Si anodes suggest that FEC and VC also improve the cycling performance of alloying anodes by forming cross-linking moieties in the SEI to improve the mechanical stability.[24−26] Other work has suggested that these additives favor the formation of components such as Li_2CO_3, and/or polycarbonates to help passivate the electrode surface more effectively.[15,43−45]

Previous work from our group has revealed that FEC and VC effectively stabilize the interface of Cu_2Sb nanowire electrodes cycled in a $LiPF_6$-based carbonate electrolyte, although it is still not entirely clear why these additives extend the cycle lifetime of Cu_2Sb so dramatically, especially VC, which resulted in the longest lifetime.[29] In the current work, the SEI formed on Cu_2Sb over different potential regions in the electrolyte with and without VC was characterized using differential capacity analysis and X-ray photoelectron spectroscopy (XPS) to better understand what types of species or functional groups in the SEI formed with VC may be beneficial for Cu_2Sb electrodes. In this study, the SEIs formed on Cu_2Sb thin film anodes in $LiClO_4$-based carbonate electrolyte solutions were examined to eliminate some variables associated with the use of $LiPF_6$-based electrolytes that could complicate the study. $LiPF_6$-based electrolytes often contain small amounts of very reactive HF, which can react with the electrolyte and SEI components and affect the SEI composition, convoluting the results.[46] Additionally, while inorganic species such as LiF are thought to passivate the electrode surface, eliminating fluorinated components from the electrolyte may help reveal what other types of organic and inorganic species are beneficial for effectively passivating the surface of intermetallic electrodes.[14,15,47]

EXPERIMENTAL SECTION

Materials. Citric acid monohydrate (Fisher Scientific, certified ACS), antimony(III) oxide nanopowder (Sb_2O_3, <250 nm, Aldrich ≥99.99%), and copper(II) nitrate hemipentahydrate ($Cu(NO_3)_2·2.5H_2O$, Aldrich ≥99.99%+) were used as received. Saturated potassium hydroxide was prepared from pellets (KOH, Fisher Scientific, Certified ACS). Phosphoric acid (H_3PO_4, 85% EMD Chemicals, ACS grade) was used to make a 2:1 (vol) H_3PO_4:H_2O solution. Ultrapure water (18 MΩ, Millipore) was used for all experiments. Dimethyl carbonate (DMC, anhydrous, ≥99%), diethyl carbonate (DEC, anhydrous, ≥99%), VC (99% with 80 ppm butylated hydroxytoluene added as stabilizer), and lithium perchlorate ($LiClO_4$, battery grade, 99.999%) were purchased from Aldrich and kept in an Ar-filled glove box without further purification. Ethylene carbonate (EC, anhydrous, Aldrich 99%) was recrystallized from ethanol, dried, and stored in an Ar-filled glove box. Lithium metal was stored in an Ar-filled glove box and cleaned prior to use by manually scraping away any surface oxide layer present to reveal the metallic Li underneath. Glass fiber separators (Whatman GF/A) were dried in an oven prior to being pumped into an Ar-filled glove box for storage and use.

Anode Preparation. Copper antimonide (Cu_2Sb) was electrodeposited at room temperature following a previously established procedure.[35] Briefly, Cu_2Sb was electrodeposited onto copper substrates (110 Cu foil, 0.002″ thick, McMaster-Carr) from a solution containing 400 mM citric acid monohydrate, 25 mM Sb_2O_3 nanopowder, and 40 mM $Cu(NO_3)_2·2.5H_2O$ and adjusted to pH 6 with saturated KOH. The Cu_2Sb films were electrodeposited at −1.05 V versus a saturated calomel electrode (SCE) onto copper substrates for 10 min at room temperature using a Gamry Reference 3000 potentiostat. The ca. 1″ × 1.5″ copper foil substrates were cleaned prior to electrodeposition by sonicating in isopropanol for 3 min to remove the organic residue, followed by electropolishing in a H_3PO_4 solution for 30 s to remove copper oxide; the substrates were then covered on one side with Kapton tape. After electrodeposition, the Cu_2Sb films were rinsed thoroughly with water, followed by isopropanol, and then dried before transferring to an Ar-filled glove box to minimize native oxide growth. The Cu_2Sb mass loading for the 10 min electrodepositions was 1.0 mg/cm^2, determined by mass difference.

Electrochemical Half-Cell Preparation and Cycling. Swagelok half cells were assembled in an Ar-filled glove box (O_2 < 1.0 ppm, H_2O < 0.5 ppm). Circular punches (1.27 cm diameter) of the electrodeposited Cu_2Sb films were sealed in the Swagelok cell body. Two polypropylene separators (Celgard, 25 μm) and a glass fiber separator, soaked in either 200 μL of 1 M $LiClO_4$ in EC/DMC/DEC (1:1:1 vol) electrolyte or 200 μL of 1 M $LiClO_4$ in EC/DMC/DEC (1:1:1 vol) with 5% (vol) VC added, were placed between the Cu_2Sb working electrode and lithium metal counter/pseudo reference electrode. All potentials in this work are referenced to the Li/Li$^+$ couple unless noted otherwise.

All half cells were cycled using an Arbin BT-2143 battery tester with an 18 h rest step before cycling. Half cells for the cycle lifetime studies were cycled galvanostatically between 0.05 and 3.0 V at a C/20 rate (ca. 15 μA/cm^2). For SEI preparation, the Cu_2Sb half cells were galvanostatically reduced from the open circuit potential (ca. 2.3 V) at a C/20 rate (ca.

https://dx.doi.org/10.1021/acs.jpcc.0c04064
J. Phys. Chem. C 2020, 124, 26083−26093

15 μA/cm^2) until a particular voltage limit was reached. Then, the current polarity was switched so that Cu_2Sb was oxidized to a higher, predetermined potential. At that point, the cells were cycled galvanostatically over that potential range for a total of 20 cycles. Three different potential regions were chosen to study SEI formation at different stages of half-cell cycling: the high potential region (HPR) between 1.8 and 3.0 V, the middle potential region (MPR) between 0.9 and 1.8 V, and the low potential region (LPR) between 0.05 and 0.9 V. For a given potential region, half cells were made using the $LiClO_4$-based electrolytes with and without VC using Cu_2Sb punches from the same film to minimize variability due to differences between films. After galvanostatic cycling was complete, the half cells had a 24 h rest step and were then dismantled in an Ar-filled glove box within 1 to 2 days of cycling completion. All electrodes were washed with 1 mL of DMC so that only the components incorporated into the SEI layer adhered to the electrode surface remained for characterization.

Characterization. XPS measurements were performed in order to analyze the chemical bonding and composition of the SEI samples using a Physical Electronics (PHI) 5800 series Multi-Technique ESCA system with a monochromatic Al Kα (hν = 1486.6 eV) source operating at 350.0 W. Samples were transferred under vacuum directly from the Ar-filled glovebox to the XPS sample introduction chamber using a custom-built sample holder so that the SEI samples were never exposed to air prior to XPS characterization.[48] Samples were pumped down for 30 min prior to characterization. An electron flood gun operating with a 5 μA emission current, 1.5 V bias voltage, and 40.0 V extractor voltage was used for charge neutralization on all SEI samples. High-resolution (HRES) spectra for the regions of interest (C 1s, Cl 2p, O 1s/Sb 3d, Li 1s, and Cu 2p) were collected sequentially with a pass energy of 23.5 eV in an interval of 0.100 eV/step. The instrument base pressure was 5 × 10^{-8} Torr or lower during data acquisition. Spectra were collected from at least 3 areas on each sample (area 126.7 mm^2) using a 0.6 mm by 2 mm spot size (area 1.2 mm^2) to ensure that any lateral heterogeneity in the SEI was accounted for. Short HRES scans were collected prior to longer acquisitions so that any sample damage could be identified, although even the longer HRES scans were relatively short (20−30 min) to avoid prolonged beam exposure and sample damage.[49] In these studies, we were interested in studying relative changes in binding energies and speciation between samples rather than obtaining absolute binding energies; therefore, all HRES spectra were shifted so that either the Cl $2p_{3/2}$ peak for ClO_4^- was located at 208.6 eV or the Cl $2p_{3/2}$ peak for Cl$^-$ was at 198.6 eV (if no ClO_4^- was detected) based on research suggesting that it is preferable to use SEI species for calibrating binding energies.[50] CasaXPS software (Version 2.3.16) was used for peak fitting and quantification of the HRES spectra. A nonlinear Shirley background and 30% Lorentzian/70% Gaussian line shape were used for peak fitting,[51] and PHI relative sensitivity factors corrected for angular distribution were used for quantification based on peak fitting. More details about the peak fitting rationale and constraints used as well as a discussion of how the XPS quantification was used in our analysis can be found in the Supporting Information.

RESULTS AND DISCUSSION

Previous studies of the effects of additives on the cycling performance of Cu_2Sb in a $LiPF_6$-based electrolyte have demonstrated that VC dramatically improves the cycle lifetime of Cu_2Sb nanowires,[29] and we have observed that it also improves the cycle lifetime of Cu_2Sb cycled in the $LiClO_4$-based electrolyte. Binder- and additive-free Cu_2Sb films ca. 1 μm thick cycle for about 15 cycles at a C/20 rate in 1 M $LiClO_4$ in EC/DEC/DMC (1:1:1 vol) electrolyte before dropping to 80% of the initial capacity. However, despite the poor performance of the Cu_2Sb films in the $LiClO_4$-based electrolyte, the addition of 5% VC improves the cycle lifetime considerably. As shown in Figure 1a, a ca. 1 μm thick Cu_2Sb film cycled over an extreme potential range (0.05−3.0 V) at a C/20 rate shows no capacity fade after 20 cycles when VC is used as an additive; in fact, it cycles for about 70 cycles before exhibiting gradual capacity fade (see Figure S1 in the Supporting Information). The Cu_2Sb film cycled with VC actually shows a slight increase in capacity after 10 cycles that is associated with electrochemical roughening or pulverization of the binder- and additive-free films that allow more of the active material to be accessed due to increased surface area.[52,53] The good capacity retention of the film cycled with VC despite electrode roughening or pulverization suggests that the SEI formed with VC has desirable mechanical properties that enable it to accommodate the large volume changes of Cu_2Sb during cycling and keep the electrode material in good contact with the current collector as it is pulverized rather than delaminating from the substrate.

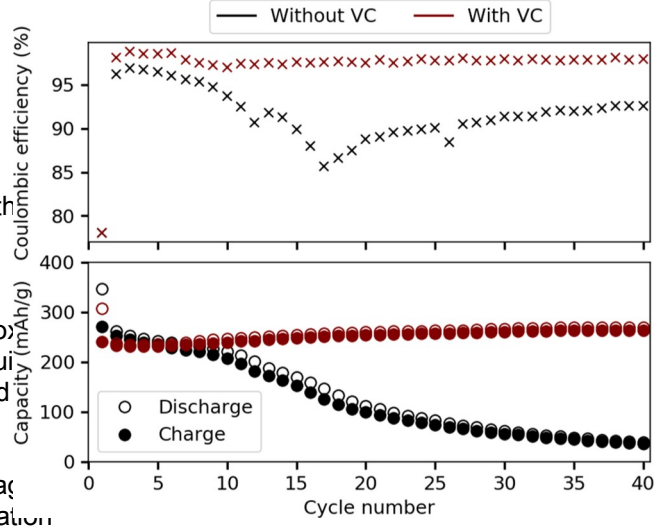

Figure 1. Coulombic efficiency and capacity data for 1 μm-thick Cu_2Sb films cycled at a C/20 rate between 0.05 and 3.0 V vs Li/Li$^+$ in the $LiClO_4$-based electrolyte with and without 5% VC added.

More insights into the failure of Cu_2Sb cycled in the $LiClO_4$-based electrolyte and the increased capacity retention associated with VC can be gained from the differential capacity plots shown in Figure 2. The intense features of the differential capacity plots corresponding to Cu_2Sb lithiation and delithiation are similar for Cu_2Sb cycled with and without VC and are in agreement with the previously reported lithium alloying and dealloying reactions of Cu_2Sb.[54,55] Looking at the much lower intensity peaks between 2.75 and 1.0 V corresponding to electrolyte reduction and SEI formation

https://dx.doi.org/10.1021/acs.jpcc.0c04064
J. Phys. Chem. C 2020, 124, 26083−26093

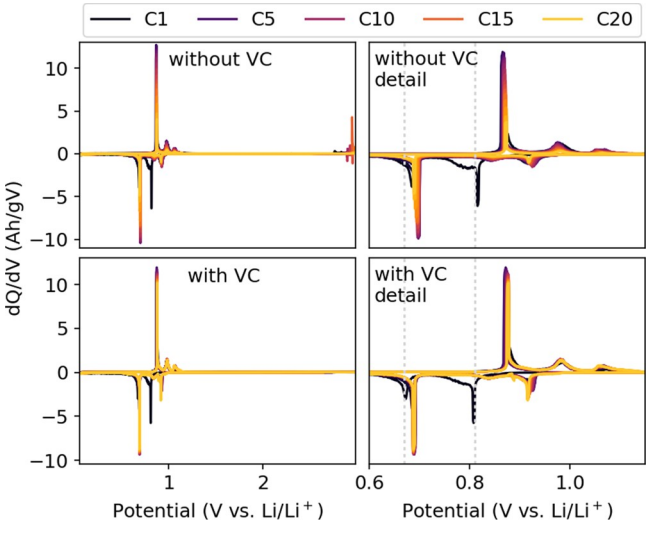

Figure 2. (Left) Full differential capacity plots for the first 20 cycles 1 μm-thick Cu_2Sb films cycled at a C/20 rate between 0.05 and 3.0 vs Li/Li^+ in the $LiClO_4$-based electrolyte with (bottom) and without (top) 5% VC added. (Right) Zoomed in differential capacity plots showing the Cu_2Sb lithiation/delithiation features from the left plots in more detail.

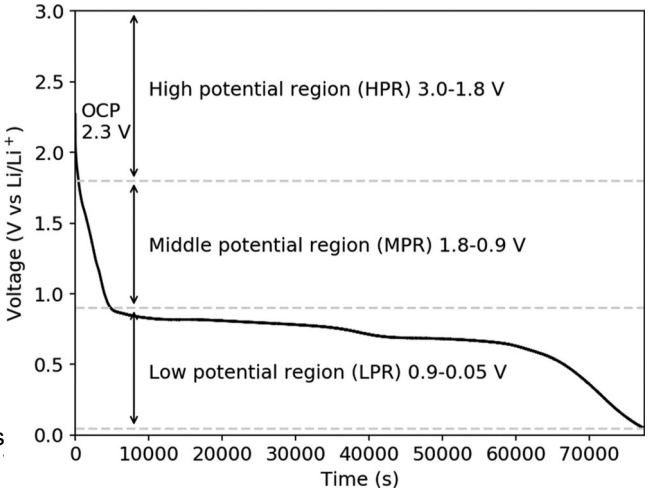

Figure 3. First cycle discharge (lithiation) of Cu_2Sb cycled with an applied current of 15 $\mu A/cm^2$. The features of the voltage profile were used to determine the potential limits for the three different regions of SEI formation chosen for this study: the HPR, MPR, and LPR.

processes in Figure S2 also reveals similarities between the samples cycled with and without VC. However, comparison of the differential capacity plots for the first 20 cycles of the Cu_2Sb half cells cycled with and without VC suggests that the failure of the film cycled without VC may be due in part to loss of electrical contact of the active material due to volume changes during lithiation/delithiation because the peaks for Cu_2Sb cycled without VC decrease in intensity with the cycle number, unlike those for Cu_2Sb cycled with VC, suggesting that for the film cycled without VC, less active material is being lithiated and delithiated with continued cycling.[56] Again, this suggests that VC may help improve the physical properties of the SEI formed on Cu_2Sb, perhaps forming a more robust SEI that is better able to withstand the large volume changes during cycling and prevent cracking and delamination of the film that result in loss of electrical contact. Additionally, there seems to be a difference in the degree of passivation of the Cu_2Sb electrodes cycled with and without VC. The first cycle lithiation peaks shown in black in Figure 2 for Cu_2Sb cycled with VC are at slightly more negative overpotentials than those for Cu_2Sb cycled without VC, especially for the phase transition at ca. 0.7 V, as demonstrated by the dotted grey lines on the right side of Figure 2. This suggests that even on the first cycle, the SEI formed on Cu_2Sb with VC is thick enough or passivating enough to slightly impede Li^+ ion transport compared to the SEI formed without VC.[56] Another striking difference between the differential capacity plots for Cu_2Sb Cu samples cycled with and without VC are the reduction and oxidation features at potentials above 2.5 V that are seen only for Cu_2Sb cycled without VC. The differences in the electrochemistry for Cu_2Sb cycled without VC suggest some sort of compositional difference between the SEIs formed with and without VC that affect the electrochemistry of the electrode material and will be discussed in further detail below.

In order to learn about the composition differences in the SEI formed from the $LiClO_4$-based electrolyte with and without VC, Cu_2Sb was electrochemically cycled over three different potential regions to target different stages of SEI formation and growth. The three different regions were chosen based on the characteristics of the voltage profile for Cu_2Sb, shown in Figure 3. The HPR, cycled between 1.8 and 3.0 V, was chosen because it is above the lithiation potential for Cu_2Sb, and there is little to no SEI formation expected in this region, so any SEI formed by cycling over this potential region may provide insights into the types of species present during the initial stages of SEI formation. The MPR, cycled between 0.9 and 1.8 V, is still higher than the Cu_2Sb lithiation potential, but based on the voltage profile, some capacity goes toward SEI formation and lithiation of surface oxides. The reported reduction potential for EC, DMC, and DEC on metallic electrodes is ca. 1.3 V, while VC reduction has been observed around 1.4 V,[57,58] and the reduction of surface oxides on Sb-based electrodes has been reported around 1.6 V.[59,60] Studying the SEI formed from cycling over the MPR is expected to provide insights into the electrolyte reactions that occur and the SEI species that are formed at higher reduction potentials. Finally, the LPR, cycled between 0.9 and 0.05 V, encompasses Cu_2Sb lithiation and is expected to provide insights into the electrolyte degradation and the types of SEI species that are formed at lower reduction potentials.

XPS was used to compare the composition and speciation of the SEIs formed over different potential regions with and without VC as an additive. Due to the heterogeneous nature of the SEI, high-resolution (HRES) XPS spectra from at least 3 different regions (1.2 mm^2 analysis area) were collected for each sample (total area 126.7 mm^2) to ensure that an accurate representation of the SEI was obtained. Representative regions for each type of SEI sample were chosen based on a combination of the spectral features and the percent atomic compositions determined from HRES peak fitting and quantification, and a more detailed description of this process can be found in the Supporting Information. The analysis regions for most of the SEI samples showed some differences in spectral features and quantification results, suggesting some lateral heterogeneity of the SEI, and two representative regions are reported for each sample to either reflect the sample heterogeneity or demonstrate the consistency between sample regions. In this set of experiments, most of the SEI samples

https://dx.doi.org/10.1021/acs.jpcc.0c04064
J. Phys. Chem. C 2020, 124, 26083−26093

were quite heterogeneous with the exception of the MPR VC SEI sample, which was relatively consistent in terms of spec features and the percent atomic composition of the sample surface.

The quantification results from the HRES peak fitting of the different SEI samples are shown in Figure 4 (see Tables S1-

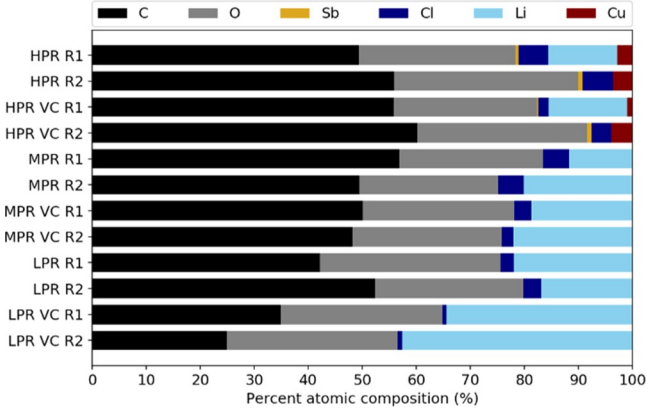

Figure 4. Percent atomic compositions for the representative regions (R1 and R2) of the SEI samples formed over different potential regions (HPR, MPR, and LPR) with and without VC, determined from XPS HRES peak fitting.

for tabulated quantification results and Figures S3−S8 for all fitted spectra). Both the HPR and HPR VC SEIs are compos primarily of C (ca. 50−60%) and O (ca. 27−34%), with only small differences in composition for the samples with and without VC, which suggests that there is SEI formation at higher potentials even though it is not readily apparent from looking at the voltage profile in Figure 1. Additionally, a small amount of Sb (ca. 0.3−0.8%) and a slightly higher amount of Cu (ca. 1−4%) were detected in these samples. In Region 1 both the HPR and HPR VC samples, a small amount of Li (c 13−15%) was detected, while for Region 2 of both samples no Li was detected. Finally, the HPR SEI formed without VC tended to be more Cl rich (ca. 6%) than the HPR VC SEI (ca 2−4%). Looking at the features of the HRES spectra we find more differences between the HPR SEIs formed with and without VC.

The Cl 2p HRES spectra are shown in Figure 5 (without fitted data for simplicity). As can be seen for the Cl 2p spectra of the HPR and HPR VC samples on the left of Figure 5, Cl $2p_{3/2}$ and $2p_{1/2}$ peaks are around 208.6 and 209.7 eV, respectively, which is indicative of a perchlorate binding environment.[61] The ClO_4^- detected at the SEI surface for both samples cycled over the HPR is from the $LiClO_4$ supporting electrolyte; since the samples were rinsed with DMC prior to XPS characterization to remove residual salt species, this suggests that the ClO_4^- is being incorporated into the SEI.

Interpretation of the O 1s/Sb 3d HRES spectra shown in Figure 6 (also presented without fitted data for clarity) is more complicated than that of the Cl 2p spectra. The reported O 1s binding energies for proposed SEI species such as lithium alkyl carbonates and lithium carbonate (Li_2CO_3) range from 531.7 to 533.8 eV,[10,17,33,62−64] and the distinguishing O 1s peak for poly VC is located around 534.5−534.7 eV.[65,66] The reported O 1s binding energies for perchlorates range from 533.0−533.6 eV.[21,61,67] This makes it difficult to distinguish different binding environments for the SEI samples even when curve

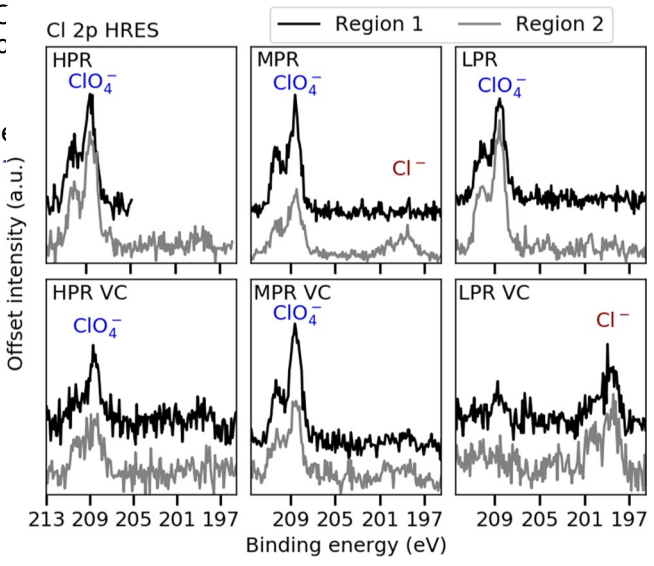

Figure 5. Cl 2p HRES spectra from the representative regions (Region 1 and Region 2) of the SEI samples formed over different potential regions (HPR, MPR, and LPR) with and without VC.

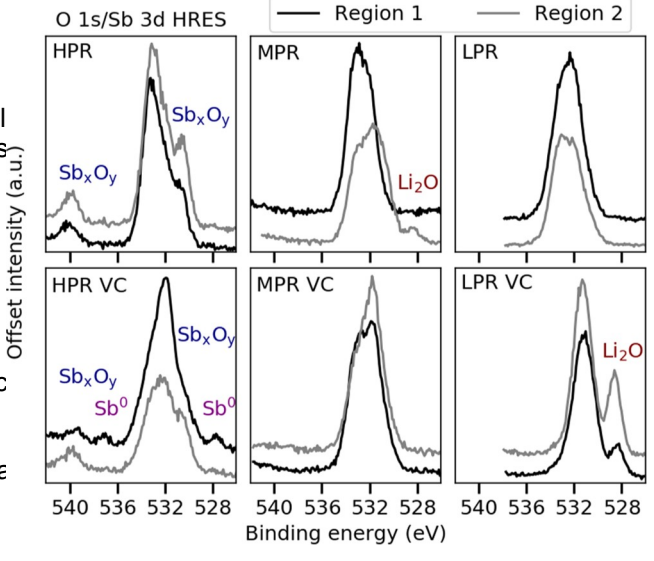

Figure 6. O 1s/Sb 3d HRES spectra from the representative regions (Region 1 and Region 2) of the SEI samples formed over different potential regions (HPR, MPR, and LPR) with and without VC.

fitting is used to deconvolute the O 1s peaks. Additionally, the binding energies of Sb $3d_{5/2}$ peaks range from ca. 528 eV for Sb^0 to 531 eV for Sb oxides, further convoluting the O 1s spectra if Sb is present.[21,59,68] However, the overlapping binding energy ranges of the O 1s and Sb 3d spectra also provide a useful way to obtain rough SEI thickness estimates. The O 1s/Sb 3d HRES spectra for pristine Sb (see Figure 6[69]) show intense Sb $3d_{5/2}$ and $3d_{3/2}$ peaks around 531.0 and 540.6 eV, respectively, for antimony oxide species from the surface oxide layer and less intense $3d_{5/2}$ and $3d_{3/2}$ peaks around 528.3 and 537.6 eV, respectively, corresponding to metallic antimony from Sb beneath the surface oxide layer. Both the HPR and HPR VC SEI samples are quite thin (<10 nm based on the information depth of XPS), as there are peaks corresponding to Sb oxide species from the surface oxide layer of the underlying Sb film for both types of samples.[69] The

https://dx.doi.org/10.1021/acs.jpcc.0c04064
J. Phys. Chem. C 2020, 124, 26083−26093

HPR VC SEI may be thinner in some regions because metallic Sb peaks are also seen for Region 1 of the HPR VC SEI sample, suggesting that the HPR VC SEI is thin enough in some regions that the metallic Sb from Cu_2Sb can be detected in addition to the Sb oxide species from the Cu_2Sb surface oxide layer.

The presence of Cu in the HPR sample set may hold one of the keys to understanding the differences between the SEIs formed with and without VC. Given the small amount of Sb detected (<1%), the comparatively large amount of Cu (ca. 1−4%) detected for the HPR and HPR VC samples is curious, one would expect the Cu amount to be roughly twice that of Sb detected if it were due to the signal from the underlying Cu_2Sb film rather 3−5 times the amount as the case here. Based on the data discussed below, it seems that the considerable amount of Cu detected is due to Cu diffusion as a result of Cu/Cu_2Sb oxidation. Even though the HPR sample set was not discharged to low enough potentials to lithiate Sb and extrude Cu out of Cu_2Sb (refer to Figure 3), it was charged to high enough potentials to result in Cu_2Sb Cu oxidation (in aqueous solutions, Cu oxidation was observed around −0.3 to 0.0 V vs SSCE depending on solution conditions, which corresponds to ca. 2.5−2.8 V vs Li/Li^+).[35] This could result in more Cu present at the surface as it is oxidized and reduced when cycling over the HPR. This is more pronounced in the HPR sample without VC, which about 3−4% Cu was detected for all regions of the sample; differential capacity analysis for the HPR SEI sample Figure 7 (top) shows the onset of an oxidation peak around 2.8 V and a reduction peak around 2.6 V that is not seen for the first discharge; these peaks are most likely due to the oxidation and reduction of Cu, respectively. There is also visual evidence to support this hypothesis, when disassembling half cells cycled up to 3.0 V in the $LiClO_4$-based electrolyte without VC, the separators are often discolored as shown in Figure S10 due to the presence of Cu as confirmed by energy dispersive X-ray spectroscopy (EDS) in Figure S11. Differential capacity analysis for the HPR VC SEI sample (Figure 7, bottom) did not show these features, this could be because there was less Cu oxidation and reduction for this sample, or not all analysis regions of the HPR VC SEI were Cu rich (ca. 1% Cu was detected for Region 1 and 4% for Region 2). Additionally, the separators from half cells cycled with VC do not show signs of discoloration due to Cu diffusion. These results suggest that the SEI formed in the presence of VC is better at protecting and passivating the Cu_2Sb surface as it seems to decrease the amount of Cu/Cu_2Sb oxidation and subsequent Cu diffusion when cycling to high potentials compared to the SEI formed without VC. Based on the XPS results for the HPR samples with and without VC, both SEIs are quite thin and nonuniform, which suggests that the differences in passivating ability are due to differences in SEI speciation rather than thickness or coverage. The features corresponding to Cu/Cu_2Sb oxidation were also seen in the differential capacity plots of Cu_2Sb cycled over the full 0.05−3 V potential range when no VC was present (Figure 2, top left plot), which suggests that even when the electrode is polarized to lower potentials, the SEI that forms does not passivate the surface well enough to prevent Cu/Cu_2Sb oxidation, unlike the SEI formed in the presence of VC, which does not show any signs of Cu/Cu_2Sb oxidation (Figure 2, bottom left plot); however, unlike for the HPR SEI cases, it is unclear at this point whether differences in passivating ability for the SEIs formed over the full voltage range are due to chemical or physical differences.

The C 1s HRES spectra may be able to provide some insights into why the SEI formed with VC may be better at protecting the Cu_2Sb surface than the SEI formed without VC since much of the SEI surfaces for both types of samples are composed of carbon. The C 1s spectra are shown in Figure 8

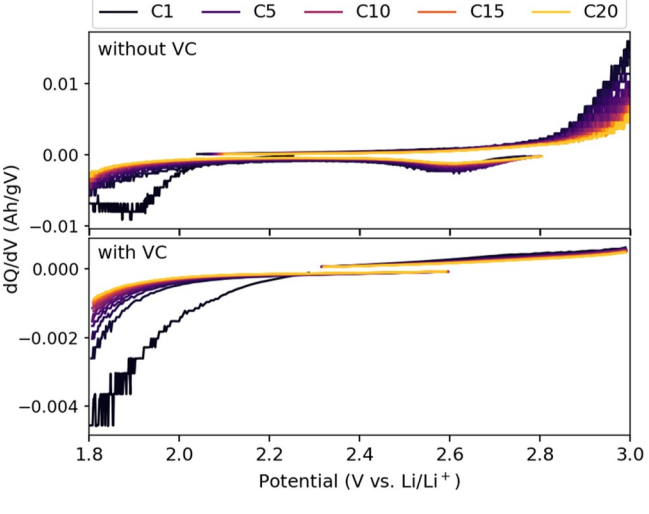

Figure 7. Comparison of the differential capacity analysis plots for the samples cycled without VC and with VC for the HPR SEI sample set.

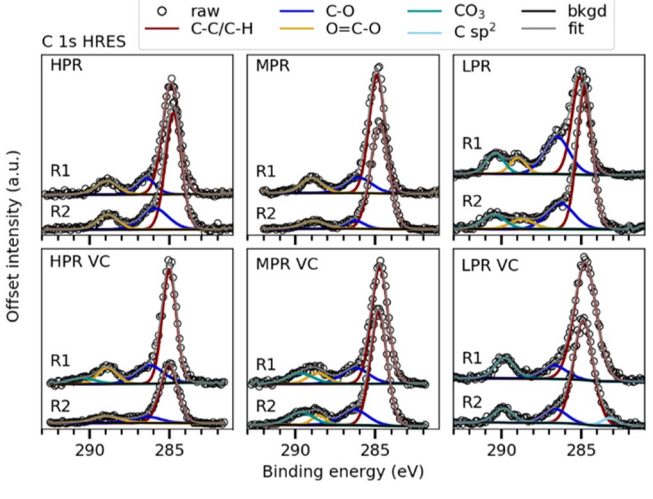

Figure 8. Fitted C 1s HRES spectra from the representative regions (R1 and R2) of the SEI samples formed over different potential regions (HPR, MPR, and LPR) with and without VC.

with the fitted data included to help illustrate differences between the spectral features for the various SEI samples. The most intense peaks in the C 1s spectra for the HPR samples with and without VC correspond to an aliphatic carbon binding environment around 285.0 eV (red peak), which could be due to some adventitious carbon in addition to organic SEI components.[33,62,63,66] Both the HPR and HPR VC samples also have a peak corresponding to a C−O binding environment around 286.5 eV (blue peak), which could be due to the presence of SEI species such as alkoxides, alkyl carbonates or carboxylates, or PEO oligomers, and a peak around 289.0 eV corresponding to an O=C−O binding environment (gold peak) that could be due to oxalates, alkyl carboxylates, or ester-

https://dx.doi.org/10.1021/acs.jpcc.0c04064
J. Phys. Chem. C 2020, 124, 26083−26093

containing species.[10,17,33,62−64,66] Based on a previous study of the SEI formed on Cu_2Sb thin film anodes in a $LiPF_6$-based electrolyte, these three C 1s binding environments may be due primarily to carboxylate and ester species, in addition to small amounts of alkoxides.[27] The most notable difference between the HPR and HPR VC SEIs is the presence of a small carbonate peak around 290.5 eV (teal peak) in Region 1 of the HPR VC SEI, which is the region where Cu_2Sb seems to be better passivated based on the lower amount of Cu detected. The carbonate peak could be due to the presence of either lithium alkyl carbonates, Li_2CO_3, or poly VC, but it seems that the presence of carbonates could be beneficial for passivation of the Cu_2Sb surface during the initial stages of cycling.[63,66] It seems most likely that the C 1s carbonate binding environment seen in the HPR VC sample is due to a species like poly VC or some other VC reduction product rather than Li alkyl carbonate species or Li_2CO_3 since those species could also be formed from the electrolyte without VC.[44,45,66,70] Because it is difficult to draw any conclusions about the carbonate species based on the XPS results alone, this warrants further exploration in future work using complementary characterization techniques such as FTIR.[44,27,45]

Both the HPR and HPR VC SEIs were quite heterogeneous, but for the MPR samples, the MPR SEI without VC was heterogeneous while the MPR VC SEI was more homogenous in terms of composition and HRES spectral features. As seen in Figure 4, the compositions of the MPR sample set (with and without VC) are quite similar, with C (48−57%) and O (26−28%) making up most of the SEI surface. The MPR VC SEI surface is quite Li rich at 19−22%, while the MPR SEI sample has Li-rich regions (20%) as well as regions with less Li (12%). The MPR VC SEI surface is made up of ca. 2−3% Cl from ClO_4^-, while the MPR SEI surface has about twice the amount of Cl at 5%, with a mixture of ClO_4^- and Cl^- seen for MPR Region 2 as shown in Figure 5 (middle column). The SEIs formed over the MPR both with and without VC are thicker than those formed over the HPR based on the absence of Sb peaks in the O 1s/Sb 3d spectra (Figure 6, middle column). Again, it is difficult to comment on differences in the O 1s spectra, but one notable feature is the presence of an O 1s peak around 528.3 eV corresponding to O^{2-} for Region 2 of the MPR SEI that is not seen for the other MPR region or for the MPR VC sample.[71] Looking at the C 1s spectra in Figure 8, both the MPR and MPR VC samples have aliphatic, C−O, and O□C−O binding environments like the HPR and HPR VC samples. The MPR VC C 1s spectrum has an additional binding environment corresponding to carbonate like Region 1 of the HPR VC sample, while no carbonate binding environment was detected at the surface of the MPR sample without VC. The intensity of the carbonate peak relative to the other C 1s peaks is higher for the MPR VC sample compared to HPR VC Region 1. This seems to reiterate that one important difference between the SEI formed without VC and with VC is the presence of carbonates, possibly in the form of poly VC or other species formed from VC reduction.[66]

Both the LPR and LPR VC SEI are also heterogeneous, and the compositions of the representative sample regions are shown in Figure 4. Like the SEIs formed with and without VC over potential regions more positive than Cu_2Sb lithiation (HPR and MPR), the SEIs formed over the LPR are composed primarily of C and O. Both the LPR and LPR VC SEI contain roughly the same amount of oxygen as the SEIs from the HPR and MPR sample sets (27−34%). However, the LPR SEI is more C-rich (42−52% C) than the LPR VC SEI (25−35% C), which contains roughly as much Li as C (34−43%). The LPR SEI is Li-rich compared to the HPR and MPR samples, but only contains about half the amount of Li as the LPR VC SEI (17−22%).

The Cl 2p and O 1s/Sb 3d spectra, shown in Figures 5 and 6 (right columns), reveal more differences between the LPR and LPR VC SEI surfaces. The LPR SEI surface is similar to the HPR and MPR SEIs in the sense that it is composed of ca. 3% Cl from ClO_4^-. In contrast, the LPR VC SEI surface is composed of only ca. 1% Cl present as LiCl.[21,67] Like the MPR SEI set, the LPR and LPR VC SEIs are thick, as no Sb 3d peaks are seen. The O 1s spectra reveal that the LPR VC sample surface contains O^{2-}, while the LPR SEI surface does not. Compared to Region 2 of the MPR SEI, which also has Li_2O, the LPR VC SEI surface contains more O^{2-} based on the intensity of the Li_2O O 1s peak relative to the intensity of the peak formed by the other O 1s binding environments at higher binding energies. The presence of a considerable amount of Li_2O on the surface of the LPR VC SEI is likely the reason that the LPR VC SEI surface is so rich in Li compared to all of the other SEI samples.

The C 1s HRES spectra in Figure 8 (right column) for the LPR sample set also highlight several differences between the SEI formed over the LPR with and without VC. Both regions of the LPR SEI sample have four C 1s binding environments corresponding to aliphatic, C−O, O□C−O, and carbonate binding environments. The C 1s spectra for both regions of the LPR VC SEI sample are notably different because they do not show a C 1s peak corresponding to an O□C−O binding environment, suggesting that the surface of the LPR VC SEI does not contain any oxalate, alkyl carboxylate, or ester species. The LPR VC SEI surface may also contain some O^{2-}, as the C 1s spectrum for Region 2 of the LPR VC sample seems to have a small lower binding energy peak around 283.0 eV, which could be due to the presence of species such as Li vinyl carbonate.[44] In the case of the LPR VC SEI surface, it seems like poly VC is not contributing to the C 1s carbonate binding environment because there is no corresponding O 1s peak around 534.5−535 eV that has been reported for poly VC.[65,66]

Carbon species make up a large percentage of the SEI surface for the samples formed over all three potential regions, both with and without VC, and the types of carbon binding environments or species present seem to play an important role in capacity retention for Cu_2Sb cycled in $LiClO_4$-based electrolytes, which has been suggested previously in studies of the SEI formed on Cu_2Sb nanowires in $LiPF_6$-based electrolytes with and without additives and for other alloying anodes such as Sn.[29,44] Based on the differences in the XPS C 1s HRES spectra for the SEI layers formed with and without VC, it seems that carbonate species in particular play an important role in SEI passivation for Cu_2Sb electrodes. The carbonate species formed from VC reduction, such as poly VC, may be necessary for passivating the Cu_2Sb surface during the early stages of cycling (prior to Cu_2Sb lithiation) in $LiClO_4$-based electrolytes and may also improve the mechanical properties of the SEI based on changes observed in the capacity over cycling. The species that form from the reduction of EC, DEC, and DMC do not seem to be sufficient for surface passivation in the $LiClO_4$-based electrolyte without VC. Based on the peaks at ca. 2.0, 1.7, and 1.2 V in the differential capacity plots for the different potential region samples (see Figures 7 and S12), the carbonate solvents are being reduced for the samples

https://dx.doi.org/10.1021/acs.jpcc.0c04064
J. Phys. Chem. C 2020, 124, 26083−26093

both with and without VC.[57,58] However, no carbonate binding environments were detected for the SEI samples formed at higher potentials (HPR and MPR) in the absence of VC; instead, species such as carboxylate salts, esters, or Li alkoxides are formed from solvent reduction based on the C 1s HRES spectra of the HPR and MPR SEI samples formed without VC. These differences in speciation for the SEIs formed without and with VC over the HPR and MPR could be due to differences in favored solvent reduction pathways or to differences in SEI reactivity based on electrode surface passivation.[42,72] In the latter case, initial solvent reduction species in the SEI formed without VC such as Li alkyl carbonates may have reacted further to form carboxylate salts, esters, or alkoxides due to poor surface passivation when VC was not used as an additive. This preliminary passivation (or lack thereof) may be particularly important for high capacity anode materials such as Cu_2Sb that experience large volume changes during cycling. Even though carbonate species are incorporated into the SEI formed without VC at lower potentials (refer to the LPR C 1s spectra in Figure 6), it does not seem to be sufficient for passivating the electrode surface, as there are still signs of Cu/Cu_2Sb oxidation when the film is cycled over the full voltage range from 0.05 to 3.0 V versus Li/Li^+ (refer to Figure 2). This electrode oxidation could be due in part to new electrode surfaces being exposed due to volume changes during cycling, but it could also be due in part to continued insufficient passivation because the Cu/Cu_2Sb oxidation features in the differential capacity plot for the VC-free sample shift to higher overpotentials with increased cycling, suggesting that continued SEI growth results in a kinetic limitation of the process but not completely preventing it. Therefore, the stage at which the beneficial species are incorporated into the SEI may be important in addition to what types of species are formed, which has also been demonstrated for tin anodes.[45] However, additional work characterizing the SEI/electrode morphology and passivating ability using techniques such as scanning electron microscopy[15,17,29,73] and redox-probe experiments,[74] respectively, is necessary to determine whether electrode volume changes and the physical properties of the SEI play a role in the differences in electrochemistry observed for the electrodes cycled over the full voltage range with and without VC in addition to the types of species present in the SEI.

Inorganic species make up a smaller percentage of the SEI surface in the samples examined in this study but may also play an important role in SEI performance and surface passivation, although based on the literature, it is still unclear whether they are beneficial for alloying anodes.[14,44,45,47,74−76] Based on comparisons of the percent atomic composition of Cl at the SEI surface due to the presence of ClO_4^- and/or Cl^- species, the SEIs formed without VC over the HPR, MPR, and LPR were more rich in Cl-containing inorganic species. While the inorganic SEI species such as LiF that are formed from electrolytes containing fluorinated components such as $LiPF_6$ or FEC are believed to be beneficial SEI components that passivate the electrode surface,[45,47,75] the presence of perchlorate in the SEI on Cu_2Sb films when $LiClO_4$-based electrolytes are used does not seem to be beneficial. Although the SEI layers formed without VC over different potential regions are quite rich in ClO_4^- compared to their VC counterparts, the SEI layers formed without VC do not passivate the Cu_2Sb surface well and Cu_2Sb oxidation has been observed when charging to 3.0 V. This suggests that not all inorganic SEI components are beneficial, and the presence of ClO_4^- in the SEI does not appear to help with surface passivation for Cu_2Sb electrodes. Chloride species and Li_2O were also detected at the surface of SEIs formed on Cu_2Sb with and without VC, but at this point, it is unclear what role Cl species and Li_2O play in the properties and performance of the SEI. The formation of both species may be undesirable since the reduction of $LiClO_4$ to form LiCl and Li_2O consumes eight moles of electrons and eight moles of Li^+.[81] The formation of LiCl and Li_2O from $LiClO_4$ reduction results in a more Li-rich SEI based on the percent atomic composition of Li for the LPR VC SEI sample, which may be beneficial for Li^+ diffusion, especially in the case of Li_2O formation.[77] The role of these two species in the passivation and properties of the SEI may warrant further investigation to better understand whether the possible improvements in surface passivation and Li^+ diffusion due to LiCl and Li_2O formation outweigh the unfavorable decrease in Li inventory.

While we have discussed the oxidation of Cu/Cu_2Sb and Cu diffusion in the context of the passivating ability of the SEI and the role of VC, we would be remiss not to also discuss the possible implications of these observations for SEI health and the capacity retention of Cu_2Sb. Without VC, charging the Cu_2Sb to high potentials results in the oxidation of Cu_2Sb to Cu and also some Cu diffusion to other parts of the cell. While metal oxidation and transport are not typically discussed in the context of alloying anodes, it is a very important area of research for cathode materials. VC has previously been found to help prevent Co oxidation in lithium cobalt oxide cathode materials.[78] Additionally, metal transport in systems containing Ni- and Mn-based cathodes has been found to have detrimental effects for the anode SEI layer, affecting the passivating ability of the SEI and exacerbating electrolyte degradation.[74,79,80] It is possible that Cu in the SEI could also play a role in the poor cycling performance observed for Cu_2Sb without VC in a couple of ways. First, the observed Cu diffusion could be playing a role in a short lifetime and rapid capacity fade of the Cu_2Sb thin film cycled without VC. If Cu diffuses away from electrode, some of the conductive Cu network that allows for good electronic conductivity in the lithiated Sb phases may no longer be present and could result in some loss of active material conductivity and cause the observed capacity fade in addition to the delamination that has been observed for Cu_2Sb cycled without VC.[81] However, this is not consistent with previous observations from our group in which Cu-deficient Cu_2Sb showed good reversibility and cycling stability.[73] Second, it is possible that the Cu species in the SEI formed without VC could be reacting with the SEI and electrolyte components, which could be another explanation for why the HPR and MPR SEI samples without VC did not contain carbonate binding environments. This explanation is more consistent with our previous observations in which Cu-rich Cu_2Sb showed large irreversible capacities and short cycle lifetimes.[73] Research on metal dissolution and transport for cathode materials has revealed that the degree of detrimental effects on the anode SEI depends on the transition metal, Mn being the most harmful for SEI health,[74,79] but it is possible that Cu could also prevent effective SEI passivation. There is precedence for Cu reactivity in other chemistry fields, as some enzymes known to react with small organic molecules contain Cu active sites.[82] This area is worth exploring further with redox probe experiments to determine the role of Cu in SEI passivation.[74] Metal transport could be an important

https://dx.doi.org/10.1021/acs.jpcc.0c04064
J. Phys. Chem. C 2020, 124, 26083−26093

consideration for other intermetallic anode materials as well, especially when Cu, a fast solid state diffuser, is used as a volume buffering component in alloying anodes.[3,4]

CONCLUSIONS

The SEI formed on Cu_2Sb thin film anodes with and without VC as an electrolyte additive was studied in order to better understand the role that VC plays in stabilizing the SEI and extending the cycle lifetime of Cu_2Sb. The cycling data (capacity vs cycle number and differential capacity analysis) suggest that some of the improvement in capacity retention observed for Cu_2Sb with VC is due to improved SEI mechanical properties, as the film cycled with VC showed evidence of electrochemical roughening but not delamination from the substrate, unlike the film cycled without VC. The SEI formed with VC also seemed to passivate the Cu_2Sb surface more effectively, as no evidence of Cu/Cu_2Sb oxidation and diffusion was observed for Cu_2Sb films cycled to oxidizing potentials with VC as an additive. The differences in the passivating ability of the SEI formed with and without VC seems to be due in part to differences in the SEI speciation.

The role that inorganic SEI components like LiF play in the passivating ability and stability of the SEI on alloying anode materials is unclear. Studying the SEI formation on Cu_2Sb without fluorinated electrolyte components allowed us to better understand what other types of organic and inorganic species may be beneficial for good SEI performance. During the initial stages of SEI formation at higher reduction potentials, the surface of the SEI formed on Cu_2Sb without VC does not contain any carbonate species, whereas the SEI surface formed with VC does. VC reduction products such as poly VC or other polycarbonate species seem to play an important role in the passivating ability of the SEI. The surface of the SEI formed without VC tended to contain more inorganic $LiClO_4$-containing species, which do not seem to passivate Cu_2Sb very effectively.

ASSOCIATED CONTENT

* Supporting Information

The Supporting Information is available free of charge at https://pubs.acs.org/doi/10.1021/acs.jpcc.0c04064.

Long term cycling data for Cu_2Sb films in the $LiClO_4$-based electrolyte; additional differential capacity analysis for Cu_2Sb cycled over the full voltage range; XPS fitting procedure and parameters; tabulated XPS fitting results; fitted HRES XPS spectra for all SEI samples; HRES XPS spectra for pristine Cu_2Sb; photographs and EDS data showing evidence of Cu diffusion; differential capacity analysis for the first discharge of the MPR and LPR SEI sample sets; and XRD of the electrodeposited Cu_2Sb film (PDF)

AUTHOR INFORMATION

Corresponding Author

Amy L. Prieto − Department of Chemistry, Colorado State University, Fort Collins, Colorado 80523, United States; orcid.org/0000-0001-9235-185X; Email: amy.prieto@colostate.edu

Authors

Leslie A. Kraynak − Department of Chemistry, Colorado State University, Fort Collins, Colorado 80523, United States

Jacob D. Schneider − Department of Chemistry, Colorado State University, Fort Collins, Colorado 80523, United States

Complete contact information is available at: https://pubs.acs.org/10.1021/acs.jpcc.0c04064

Author Contributions

The manuscript was written through contributions of all authors. All authors have given approval to the final version of the manuscript.

Funding

NSF SSMC (SSMC-1710672).

Notes

The authors declare no competing financial interest.

ACKNOWLEDGMENTS

This work was supported by the NSF SSMC program (SSMC-1710672). The authors would also like to thank the Central Instrument Facility staff at Colorado State University, in particular Dr. Patrick McCurdy, for assistance with XPS. We would also like to thank Dr. Timothy S. Arthur and Dr. Matthew T. Rawls for their contributions to initial SEI potential region studies in the group. Finally, we would also like to thank Dr. Maxwell C. Schulze, Dr. Daniel B. Agocs, and Nathan Gimble for the helpful feedback on earlier versions of this manuscript.

REFERENCES

(1) Choi, J. W.; Aurbach, D. Promise and Reality of Post-Lithium-Ion Batteries with High Energy Densities. Nat. Rev. Mater. 2016, 1, 16013.

(2) Obrovac, M. N.; Chevrier, V. L. Alloy Negative Electrodes for Li-Ion Batteries. Chem. Rev. 2014, 114, 11444−11502.

(3) Zhang, W.-J. Review of the Electrochemical Performance of Alloy Anodes for Lithium-Ion Batteries. J. Power Sources 2011, 196, 13−24.

(4) Thackeray, M. M.; Vaughey, J. T.; Johnson, C. S.; Kropf, A. J.; Benedek, R.; Fransson, L. M. L.; Edström, K. Structural Considerations of Intermetallic Electrodes for Lithium Batteries. J. Power Sources 2003, 113, 124−130.

(5) Winter, M. The Solid Electrolyte Interphase-The Most Important and the Least Understood Solid Electrolyte in Rechargeable Li Batteries. Z. Phys. Chem. 2009, 223, 1395−1406.

(6) Verma, P.; Maire, P.; Novák, P. A Review of the Features and Analyses of the Solid Electrolyte Interphase in Li-Ion Batteries. Electrochim. Acta 2010, 55, 6332−6341.

(7) Goodenough, J. B.; Kim, Y. Challenges for Rechargeable Li Batteries. Chem. Mater. 2010, 22, 587−603.

(8) Xu, K. Nonaqueous Liquid Electrolytes for Lithium-Based Rechargeable Batteries. Chem. Rev. 2004, 104, 4303−4418.

(9) Tokranov, A.; Kumar, R.; Li, C.; Minne, S.; Xiao, X.; Sheldon, B. W. Control and Optimization of the Electrochemical and Mechanical Properties of the Solid Electrolyte Interphase on Silicon Electrodes in Lithium Ion Batteries. Adv. Energy Mater. 2016, 6, 1502302−12.

(10) Schroder, K. W.; Celio, H.; Webb, L. J.; Stevenson, K. J. Examining Solid Electrolyte Interphase Formation on Crystalline Silicon Electrodes: Influence of Electrochemical Preparation and Ambient Exposure Conditions. J. Phys. Chem. C 2012, 116, 19737−19747.

(11) Nie, M.; Lucht, B. L. Role of Lithium Salt on Solid Electrolyte Interface (SEI) Formation and Structure in Lithium Ion Batteries. J. Electrochem. Soc. 2014, 161, A1001−A1006.

(12) Jurng, S.; Brown, Z. L.; Kim, J.; Lucht, B. L. Effect of Electrolyte on the Nanostructure of the Solid Electrolyte Interphase

(SEI) and Performance of Lithium Metal Anodes. Energy Environ. Sci. 2018, 11, 2600−2608.
(13) Leroy, S.; Martinez, H.; Dedryvère, R.; Lemordant, D.; Gonbeau, D. Influence of the Lithium Salt Nature over the Surface Film Formation on a Graphite Electrode in Li-Ion Batteries: An XPS Study. Appl. Surf. Sci. 2007, 253, 4895−4905.
(14) Yoon, T.; Chapman, N.; Seo, D. M.; Lucht, B. L. Lithium Salt Effects on Silicon Electrode Performance and Solid Electrolyte Interphase (SEI) Structure, Role of Solution Structure on SEI Formation. J. Electrochem. Soc. 2017, 164, A2082−A2088.
(15) Nguyen, C. C.; Lucht, B. L. Comparative Study of Fluoroethylene Carbonate and Vinylene Carbonate for Silicon Anodes in Lithium Ion Batteries. J. Electrochem. Soc. 2014, 161, A1933−A1938.
(16) Wagner, M. R.; Raimann, P. R.; Trifonova, A.; Moeller, K.-C.; Besenhard, J. O.; Winter, M. Electrolyte Decomposition Reactions on Tin- and Graphite-Based Anodes: Are Different. Electrochem. Solid-State Lett. 2004, 7, A201−A205.
(17) Chan, C. K.; Ruffo, R.; Hong, S. S.; Cui, Y. Surface Chemistry and Morphology of the Solid Electrolyte Interphase on Silicon Nanowire Lithium-Ion Battery Anodes. J. Power Sources 2009, 189, 1132−1140.
(18) Vogl, U. S.; Lux, S. F.; Das, P.; Weber, A.; Placke, T.; Kostecki, R.; Winter, M. The Mechanism of SEI Formation on Single Crystal Si(100), Si(110) and Si(111) Electrodes. J. Electrochem. Soc. 2015, 162, A2281−A2288.
(19) Fransson, L.; Eriksson, T.; Edström, K.; Gustafsson, T.; Thomas, J. O. Influence of Carbon Black and Binder on Li-Ion Batteries. J. Power Sources 2001, 101, 1−9.
(20) Jaumann, T.; Balach, J.; Klose, M.; Oswald, S.; Langklotz, U.; Michaelis, A.; Eckert, J.; Giebeler, L. SEI-Component Formation on Sub 5 Nm Sized Silicon Nanoparticles in Li-Ion Batteries: The Role of Electrode Preparation, FEC Addition and Binder. Phys. Chem. Chem. Phys. 2015, 17, 24956−24967.
(21) Bodenes, L.; Darwiche, A.; Monconduit, L.; Martinez, H. The Solid Electrolyte Interphase a Key Parameter of the High Performance of Sb in Sodium-Ion Batteries: Comparative X-Ray Photoelectron Spectroscopy Study of Sb/Na-Ion and Sb/Li-Ion Batteries. J. Power Sources 2015, 273, 14−24.
(22) Bryngelsson, H.; Stjerndahl, M.; Gustafsson, T.; Edström, K. How Dynamic Is the SEI? J. Power Sources 2007, 174, 970−975.
(23) Winter, M.; Appel, W. K.; Evers, B.; Hodal, T.; Möller, K.-C.; Schneider, I.; Wachtler, M.; Wagner, M. R.; Wrodnigg, G. H.; Besenhard, J. O. Studies on the Anode/Electrolyte Interface in Lithium Ion Batteries. Monatsh. Chem. 2001, 132, 473−486.
(24) Jin, Y.; Kneusels, N.-J. H.; Magusin, P. C. M. M.; Kim, G.; Castillo-Martínez, E.; Marbella, L. E.; Kerber, R. N.; Howe, D. J.; Paul, S.; Liu, T.; et al. Identifying the Structural Basis for the Increased Stability of the Solid Electrolyte Interphase Formed on Silicon with the Additive Fluoroethylene Carbonate. J. Am. Chem. Soc. 2017, 139, 14992−15004.
(25) Jin, Y.; Kneusels, N.-J. H.; Marbella, L. E.; Castillo-Martínez, E.; Magusin, P. C. M. M.; Weatherup, R. S.; Jónsson, E.; Liu, T.; Paul, S.; Grey, C. P. Understanding Fluoroethylene Carbonate and Vinylene Carbonate Based Electrolytes for Si Anodes in Lithium Ion Batteries with NMR Spectroscopy. J. Am. Chem. Soc. 2018, 140, 9854−9867.
(26) Shkrob, I. A.; Wishart, J. F.; Abraham, D. P. What Makes Fluoroethylene Carbonate Different? J. Phys. Chem. C 2015, 119, 14954−14964.
(27) Song, S.-W.; Reade, R. P.; Cairns, E. J.; Vaughey, J. T.; Thackeray, M. M.; Striebel, K. A. Cu2Sb Thin-Film Electrodes Prepared by Pulsed Laser Deposition for Lithium Batteries. J. Electrochem. Soc. 2004, 151, A1012−A1019.
(28) Allcorn, E.; Manthiram, A. Thermal Stability of Sb and Cu2Sb Anodes in Lithium-Ion Batteries. J. Electrochem. Soc. 2015, 162, A1778−A1786.
(29) Jackson, E. D.; Prieto, A. L. Copper Antimonide Nanowire Array Lithium Ion Anodes Stabilized by Electrolyte Additives. ACS Appl. Mater. Interfaces 2018, 8, 30379−30386.
(30) Vaughey, J. T.; Johnson, C. S.; Kropf, A. J.; Benedek, R.; Thackeray, M. M.; Tostmann, H.; Sarakonsri, T.; Hackney, S.; Fransson, L.; Edström, K.; et al. Structural and Mechanistic Features of Intermetallic Materials for Lithium Batteries. Power Sources 2001, 97−98, 194−197.
(31) Ehinon, K. K. D.; Naille, S.; Dedryvère, R.; Lippens, P.-E.; Jumas, J.-C.; Gonbeau, D. Ni3Sn4 Electrodes for Li-Ion Batteries: Li-Sn Alloying Process and Electrode/Electrolyte Interface Phenomena. Chem. Mater. 2008, 20, 5388−5398.
(32) Naille, S.; Dedryvère, R.; Martinez, H.; Leroy, S.; Lippens, P.-E.; Jumas, J.-C.; Gonbeau, D. XPS Study of Electrode/Electrolyte Interfaces of η-Cu6Sn5 Electrodes in Li-Ion Batteries. J. Power Sources 2007, 174, 1086−1090.
(33) Stjerndahl, M.; Bryngelsson, H.; Gustafsson, T.; Vaughey, J. T.; Thackeray, M. M.; Edström, K. Surface Chemistry of Intermetallic AlSb-Anodes for Li-Ion Batteries. Electrochim. Acta 2007, 52, 4947−4955.
(34) Lahiri, A.; Endres, F. Review □ Electrodeposition of Nanostructured Materials from Aqueous, Organic and Ionic Liquid Electrolytes for Li-Ion and Na-Ion Batteries: A Comparative Review. J. Electrochem. Soc. 2017, 164, D597−D612.
(35) Mosby, J. M.; Prieto, A. L. Direct Electrodeposition of Cu2Sb for Lithium-Ion Battery Anodes. J. Am. Chem. Soc. 2008, 130, 10656−10661.
(36) Kim, I.-S.; Vaughey, J. T.; Auciello, O. Thin-Film Cu(6)Sn(5) Electrodes: Synthesis, Properties, and Current Collector Interactions. J. Electrochem. Soc. 2008, 155, A448−A451.
(37) Chusid, O. Y.; Ely, Y. E.; Aurbach, D.; Babai, M.; Carmeli, Y. Electrochemical and Spectroscopic Studies of Carbon Electrodes in Lithium Battery Electrolyte Systems. J. Power Sources 1993, 43, 47−64.
(38) Michan, A. L.; Leskes, M.; Grey, C. P. Voltage Dependent Solid Electrolyte Interphase Formation in Silicon Electrodes: Monitoring the Formation of Organic Decomposition Products. Chem. Mater. 2016, 28, 385−398.
(39) Perre, E.; Taberna, P. L.; Mazouzi, D.; Poizot, P.; Gustafsson, T.; Edström, K.; Simon, P. Electrodeposited Cu2Sb as Anode Material for 3-Dimensional Li-Ion Microbatteries. J. Mater. Res. 2010, 25, 1485−1491.
(40) Zhang, S. S. A Review on Electrolyte Additives for Lithium-Ion Batteries. J. Power Sources 2006, 162, 1379−1394.
(41) Haregewoin, A. M.; Wotango, A. S.; Hwang, B.-J. Electrolyte Additives for Lithium Ion Battery Electrodes: Progress and Perspectives. Energy Environ. Sci. 2016, 9, 1955−1988.
(42) Ushirogata, K.; Sodeyama, K.; Okuno, Y.; Tateyama, Y. Additive Effect on Reductive Decomposition and Binding of Carbonate-Based Solvent toward Solid Electrolyte Interphase Formation in Lithium-Ion Battery. J. Am. Chem. Soc. 2013, 135, 11967−11974.
(43) Zhang, W.; Ghamouss, F.; Darwiche, A.; Monconduit, L.; Lemordant, D.; Dedryvère, R.; Martinez, H. Surface Film Formation on TiSnSb Electrodes: Impact of Electrolyte Additives. J. Power Sources 2014, 268, 645−657.
(44) Park, S.; Heon Ryu, J.; Oh, S. M. Passivating Ability of Surface Film Derived from Vinylene Carbonate on Tin Negative Electrode. Electrochem. Soc. 2011, 158, A498−A503.
(45) Seo, D. M.; Nguyen, C. C.; Young, B. T.; Heskett, D. R.; Woicik, J. C.; Lucht, B. L. Characterizing Solid Electrolyte Interphase on Sn Anode in Lithium Ion Battery. J. Electrochem. Soc. 2015, 162, A7091−A7095.
(46) Aurbach, D.; Markovsky, B.; Shechter, A.; Ein-Eli, Y.; Cohen, H. A Comparative Study of Synthetic Graphite and Li Electrodes in Electrolyte Solutions Based on Ethylene Carbonate Dimethyl Carbonate Mixtures. J. Electrochem. Soc. 1996, 143, 3809−3820.
(47) Chan, A. K.; Tatara, R.; Feng, S.; Karayaylali, P.; Lopez, J.; Stephens, I. E. L.; Shao-Horn, Y. Concentrated Electrolytes for Enhanced Stability of Al-Alloy Negative Electrodes in Li-Ion Batteries. J. Electrochem. Soc. 2019, 166, A1867−A1874.

https://dx.doi.org/10.1021/acs.jpcc.0c04064
J. Phys. Chem. C 2020, 124, 26083−26093

(48) Schneider, D.; Agocs, D. B.; Prieto, A. L. Design of a Sample Transfer Holder to Enable Air-Free X-Ray Photoelectron Spectroscopy. Chem. Mater. 2020, 32, 8091.
(49) Philippe, B.; Hahlin, M.; Edström, K.; Gustafsson, T.; Siegbahn, H.; Rensmo, H. Photoelectron Spectroscopy for Lithium Battery Interface Studies. J. Electrochem. Soc. 2016, 163, A178−A191.
(50) Lindgren, F.; Rehnlund, D.; Källquist, I.; Nyholm, L.; Edström, K.; Hahlin, M.; Maibach, J. Breaking Down a Complex System: Interpreting PES Peak Positions for Cycled Li-Ion Battery Electrodes. J. Phys. Chem. C 2017, 121, 27303−27312.
(51) Sherwood, P. M. A. The Use and Misuse of Curve Fitting in the Analysis of Core X-Ray Photoelectron Spectroscopic Data. Surf. Interface Anal. 2019, 51, 589−610.
(52) Antitomaso, P.; Fraisse, B.; Stievano, L.; Biscaglia, S.; Ayme-Perrot, D.; Girard, P.; Sougrati, M. T.; Monconduit, L. SnSb Electrodes for Li-Ion Batteries: The Electrochemical Mechanism and Capacity Fading Origins Elucidated by Using Operando Techniques. J. Mater. Chem. A 2017, 5, 6546−6555.
(53) Schulze, M. C.; Schulze, R. K.; Prieto, A. L. Electrodeposited Thin-Film CuxSb Anodes for Li-Ion Batteries: Enhancement of Cycle Life via Tuning of Film Composition and Engineering of the Film-Substrate Interface. J. Mater. Chem. A 2018, 6, 12708−12717.
(54) Matsuno, S.; Noji, M.; Kashiwagi, T.; Nakayama, M.; Wakihara, M. Construction of the Ternary Phase Diagram for the Li-Cu-Sb System as the Anode Material for a Lithium Ion Battery. J. Phys. Chem. C 2007, 111, 7548−7553.
(55) Fransson, L. M. L.; Vaughey, J. T.; Benedek, R.; Edström, K.; Thomas, J. O.; Thackeray, M. M. Phase Transitions in Lithiated Cu2Sb Anodes for Lithium Batteries: An in Situ X-Ray Diffraction Study. Electrochem. Commun. 2001, 3, 317−323.
(56) Smith, A. J.; Dahn, J. R. Delta Differential Capacity Analysis. J. Electrochem. Soc. 2012, 159, A290−A293.
(57) Haregewoin, A. M.; Leggesse, E. G.; Jiang, J.-C.; Wang, F.-M.; Hwang, B.-J.; Lin, S. D. Comparative Study on the Solid Electrolyte Interface Formation by the Reduction of Alkyl Carbonates in Lithium Ion Battery. Electrochim. Acta 2014, 136, 274−285.
(58) Zhang, X.; Kostecki, R.; Richardson, T. J.; Pugh, J. K.; Ross, P. N. Electrochemical and Infrared Studies of the Reduction of Organic Carbonates. J. Electrochem. Soc. 2001, 148, A1341−A1345.
(59) Bryngelsson, H.; Eskhult, J.; Nyholm, L.; Herranen, M.; Alm, O.; Edström, K. Electrodeposited Sb and Sb/Sb2O3 Nanoparticle Coatings as Anode Materials for Li-Ion Batteries. Chem. Mater. 2007, 19, 1170−1180.
(60) Bryngelsson, H.; Eskhult, J.; Nyholm, L.; Edström, K. Thin Films of Cu2Sb and Cu9Sb2 as Anode Materials in Li-Ion Batteries. Electrochim. Acta 2008, 53, 7226−7234.
(61) Beard, B. C. Sodium Salts of Chlorine Oxyacid Anions, Cl(+7) Perchlorate, XPS Comparison Spectra. Surf. Sci. Spectra 1992, 2, 97−103.
(62) Dedryvère, R.; Laruelle, S.; Grugeon, S.; Gireaud, L.; Tarascon, J.-M. M.; Gonbeau, D. XPS Identification of the Organic and Inorganic Components of the Electrode/Electrolyte Interface Formed on a Metallic Cathode. J. Electrochem. Soc. 2005, 152, A689−A696.
(63) Dedryvère, R.; Gireaud, L.; Grugeon, S.; Laruelle, S.; Tarascon, J.-M.; Gonbeau, D. Characterization of Lithium Alkyl Carbonates by X-Ray Photoelectron Spectroscopy: Experimental and Theoretical Study. J. Phys. Chem. B 2005, 109, 15868−15875.
(64) Li, J.-T.; Swiatowska, J.; Seyeux, A.; Huang, L.; Maurice, V.; Sun, S.-G.; Marcus, P. XPS and ToF-SIMS Study of Sn − Co Alloy Thin Films as Anode for Lithium Ion Batteries. J. Power Sources 2010, 195, 8251−8257.
(65) El Ouatani, L.; Dedryvère, R.; Siret, C.; Biensan, P.; Gonbeau, D. Effect of Vinylene Carbonate Additive in Li-Ion Batteries: Comparison of LiCoO2/C, LiFePO4/C, and LiCoO2/Li4Ti5O12 Systems. J. Electrochem. Soc. 2009, 156, A468−A477.
(66) El Ouatani, L.; Dedryvère, R.; Siret, C.; Biensan, P.; Reynaud, S.; Iratçabal, P.; Gonbeau, D. The Effect of Vinylene Carbonate Additive on Surface Film Formation on Both Electrodes in Li-Ion Batteries. J. Electrochem. Soc. 2009, 156, A103−A113.
(67) Morgan, W. E.; Van Wazer, J. R.; Stec, W. J. Inner-Orbital Photoelectron Spectroscopy of the Alkali Metal Halides, Perhalates, Phosphates, and Pyrophosphates. J. Am. Chem. Soc. 1973, 95, 751−755.
(68) Garbassi, F. XPS and AES Study of Antimony Oxides. Surf. Interface Anal. 1980, 2, 165−169.
(69) James, T. L. Photoelectron Spectroscopy. J. Chem. Educ. 1971, 48, 712−718.
(70) Ota, H.; Sakata, Y.; Inoue, A.; Yamaguchi, S. Analysis of Vinylene Carbonate Derived SEI Layers on Graphite Anode. J. Electrochem. Soc. 2004, 151, A1659−A1669.
(71) Shiraishi, S.; Kanamura, K.; Takehara, Z. I. Influence of Initial Surface Condition of Lithium Metal Anodes on Surface Modification with HF. J. Appl. Electrochem. 1999, 29, 869−881.
(72) Tavassoli, H.; Buthker, J. W.; Ferguson, G. A.; Curtiss, L. A.; Gewirth, A. A. Solvent Oligomerization during SEI Formation on Model Systems for Li-Ion Battery Anodes. J. Electrochem. Soc. 2012, 159, A730−A738.
(73) Jackson, E. D.; Mosby, J. M.; Prieto, A. L. Evaluation of the Electrochemical Properties of Crystalline Copper Antimonide Thin Film Anodes for Lithium Ion Batteries Produced by Single Step Electrodeposition. Electrochim. Acta 2016, 214, 253−264.
(74) Harris, O. C.; Tang, M. H. Molecular Probes Reveal Chemical Selectivity of the Solid-Electrolyte Interphase. J. Phys. Chem. C 2018, 122, 20632−20641.
(75) Qiao, R.; Lucas, I. T.; Karim, A.; Syzdek, J.; Liu, X.; Chen, W.; Persson, K.; Kostecki, R.; Yang, W. Distinct Solid-Electrolyte-Interphases on Sn (100) and (001) Electrodes Studied by Soft X-Ray Spectroscopy. Adv. Mater. Interfaces 2014, 1, 1300115.
(76) Ulus, A.; Rosenberg, Y.; Burstein, L.; Peled, E. Tin Alloy-Graphite Composite Anode for Lithium-Ion Batteries. J. Electrochem. Soc. 2002, 149, A635−A643.
(77) Chen, Y. C.; Ouyang, C. Y.; Song, L. J.; Sun, Z. L. Electrical and Lithium Ion Dynamics in Three Main Components of Solid Electrolyte Interphase from Density Functional Theory Study. J. Phys. Chem. C 2011, 115, 7044−7049.
(78) Takamatsu, D.; Orikasa, Y.; Mori, S.; Nakatsutsumi, T.; Yamamoto, K.; Koyama, Y.; Minato, T.; Hirano, T.; Tanida, H.; Arai, H.; et al. Effect of an Electrolyte Additive of Vinylene Carbonate on the Electronic Structure at the Surface of a Lithium Cobalt Oxide Electrode under Battery Operating Conditions. Phys. Chem. C 2015, 119, 9791−9797.
(79) Solchenbach, S.; Hong, G.; Freiberg, A. T. S.; Jung, R.; Gasteiger, H. A. Electrolyte and SEI Decomposition Reactions of Transition Metal Ions Investigated by On-Line Electrochemical Mass Spectrometry. J. Electrochem. Soc. 2018, 165, A3304−A3312.
(80) Joshi, T.; Eom, K.; Yushin, G.; Fuller, T. F. Effects of Dissolved Transition Metals on the Electrochemical Performance and SEI Growth in Lithium-Ion Batteries. J. Electrochem. Soc. 2014, 161, A1915−A1921.
(81) Trahey, L.; Kung, H. H.; Thackeray, M. M.; Vaughey, J. T. Effect of Electrode Dimensionality and Morphology on the Performance of Cu2Sb Thin Film Electrodes for Lithium-Ion Batteries. Eur. J. Inorg. Chem. 2011, 2011, 3984−3988.
(82) Doerrer, L. H. Cu in Biology: Unleashed by O-2 and Now Irreplaceable. Inorg. Chim. Acta 2018, 481, 4−24.

https://dx.doi.org/10.1021/acs.jpcc.0c04064
J. Phys. Chem. C 2020, 124, 26083−26093